Toward High-Spatial Resolution Gravity Surveying of the Mid-Ocean Ridges with Autonomous Underwater Vehicles

James C. Kinsey*, Maurice A. Tivey† and Dana R. Yoerger*

*Department of Applied Ocean Physics and Engineering
†Department of Geology and Geophysics
Woods Hole Oceanographic Institution, Woods Hole, MA USA
{jkinsey,mtivey,dyoerger}@whoi.edu

***Abstract*— The shallow ocean crust of the mid-ocean ridge (MOR) is a critical environment where important chemical and biological exchanges occur. Resolving the 3-D structure of the subsurface environment beneath MOR crests at spatial scales ranging from 1-1000 meters remains a continuing challenge in marine geophysics. Previous submerged gravity surveys have employed manned, remotely operated, or towed submersibles — to date, autonomous underwater vehicles (AUVs) have not been used. Obtaining sub-mGal gravity measurements requires highly accurate knowledge of vehicle depth, velocity, attitude, and attitude rate, and we report the impact that sensing errors have on obtaining accurate estimates of the vehicle acceleration measured by the gravimeter. We investigate the effect of AUV velocity on filtering of the gravity anomaly data and how this bounds the achievable spatial resolution of gravity surveys. These results demonstrate the limitations imposed on continuous gravity surveying by vehicle velocity and present navigation sensing. Precision gravimetry will significantly enhance the bathymetric, magnetic, and optical data currently obtained by the AUV, and the data obtained promises to advance our knowledge of a wide variety of processes occurring at MORs, as well as other structurally complex seafloor terrains.**

I. INTRODUCTION

Oceanic crust produced at the mid-ocean ridge (MOR) has a sub-seafloor environment that hosts important chemical, geophysical, and biological processes. Techniques such as near-bottom bathymetric sonar and optical imaging enable mapping the seafloor with centimeter precision; however, with the possible exception of magnetism, most techniques for resolving sub-seafloor structure possess significantly poorer spatial resolution. The paucity of sub-mGal ($10^{-5}m/s^2$) high-resolution spatially-dense measurements of the sub-seafloor environment impedes our understanding of MOR processes that occur over spatial scales ranging from 10-1000 meters — such as dike emplacement [4], [10], [31], hydrothermal vent fluid circulation [10], [31], and mineral deposits. This paper discusses employing AUVs for gravity surveying — the measurement of gravity anomalies resulting from density variations in the upper oceanic crust — with sufficient spatial resolution to characterize small-scale density changes in the shallow crust. Developing fine-spatial resolution near-bottom gravity surveying capable of resolving meter-scale sub-seafloor structure would provide an improved understanding of the 3-D structure of the shallow crust and elucidate processes occurring at MORs.

An example of how near-bottom fine-spatial resolution gravity data in MOR crestal terrains could be used to better understand crustal structure can be shown for the Main Endeavor hydrothermal vent Field (MEF) located on the Juan de Fuca Ridge. Multibeam bathymetric sonar and three-axis magnetometer surveys provide an intriguing view of how sub-seafloor structure at this site has been impacted by hydrothermal fluid flow (Figure 1). The Bastille and Dante-Grotto vents are separated by 200m and the magnetic data suggests independent upflow zones beneath the two vent systems [27]. High-resolution magnetic surveys provide only a partial picture of the sub-seafloor structure. Augmenting these magnetic measurements with near-bottom gravity data of comparable spatial resolution would significantly advance our ability to define the geometry and depth extent of these processes. For example, we modeled two cases for a hypothetical gravity survey of the MEF.

Support for this research provided by the WHOI Deep Ocean Exploration Institute and a WHOI Green Innovation Technology Award.

We assumed a vertical cylinder of 50 m radius, extending to infinite depth, measured at an altitude of 20m. The first case assumes that the crust contained within the cylinder is partially impacted by 350C hydrothermal vent fluid, resulting in a negative density contrast between the impacted and surrounding crust. This contrast results in gravity reduction on the order of 1 mGal (red line, Fig. 2, top plot). The second case assumes that metal sulfide precipitation is occurring within the cylinder-contained crust, resulting in a positive density contrast and producing a gravity increase on the order of 1 mGal (blue line Fig. 2, top plot). This simple model underscores how near bottom gravimetry, along with other remote-sensing techniques, can provide a more comprehensive picture of the subsurface structure of hydrothermal upflow zones.

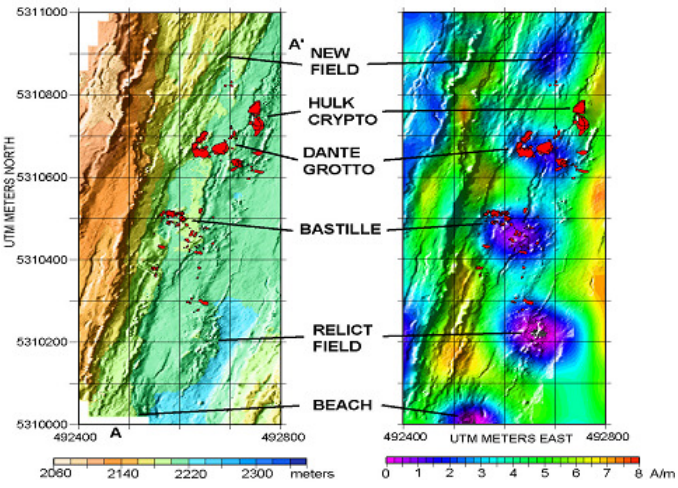

Fig. 1. Left panel shows seafloor micro-bathymetry of the MEF with red areas showing the main vent locations. Right panel shows crustal-magnetization — note the correlation of circular magnetization lows with active and inactive vent areas (from [27]).

This paper discusses using AUVs to conduct precise spatially-dense gravity surveys. Section II reviews previously reported near-bottom gravity surveys and Section II-A discusses the challenges associated with high-precision underway gravity surveying. The potential of AUVs for submerged gravity surveying is presented in Section III. Section IV introduces a two-dimensional gravity model of the TAG hydrothermal vent field and discusses some of the vehicle control and navigation challenges associated with underway surveying and identifies practical limits for when on-bottom surveying must be used *in-lieu* of underway surveying.

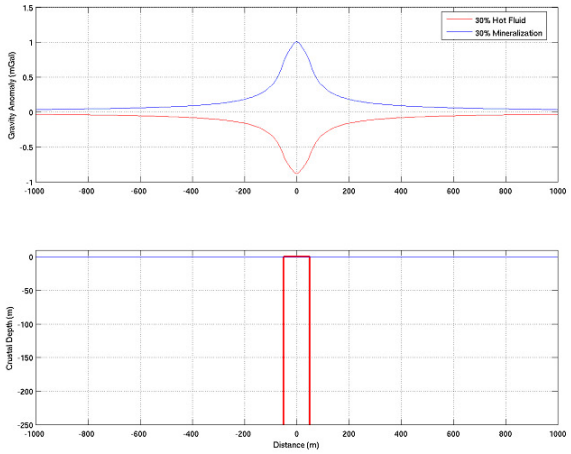

Fig. 2. Simulated results of two possible scenarios for a gravity survey over an upflow zone (modeled as a cylinder 50m in radius and infinitely deep, lower plot) at the MEF. The first case assumes the upflow zone is composed of 70% basalt and 30% hot hydrothermal vent fluid for a composite density of $2061 kg/m^3$ lower than the density of the surrounding crust containing 100% basalt. The result is a gravity reduction (red line in top plot). The second case assumes the upflow zone is composed of 70% basalt and 30% mineralization for a composite density of $3369 kg/m^3$. The result is an increased gravity signal (blue line in top plot).

II. Previous Work

To date, near-bottom gravity surveys have primarily employed a seafloor technique in which a human occupied vehicle (HOV) periodically lands on the bottom and a land gravimeter is used inside the vehicle to measure gravity. Luyendyk employed a Lacoste-Romberg gravimeter inside the *Alvin* submersible to survey a cross-section of the EPR at 21°N, and speculated that the anomalies in the data result from hydrothermal circulation of warm seawater in the shallow crust [18]. A similar result was obtained at the TAG hydrothermal mound, where low apparent density may reflect the presence of abundant anhydrite and/or substantial fluid flow within the mound [5]. Numerous HOV gravity surveys of the Juan de Fuca Ridge have been conducted [8], [9], [13], [15], [21] and find that gravity anomalies occur because of the alteration of crust, the occurrence of significant porosity at faults bounding the rift valley of the MOR at Endeavour ridge, and from the lithological contrasts in oceanic crust exposed at a transform fault.

On-bottom gravity surveys have also been conducted using gravimeters placed on the seafloor. Hildebrand and colleagues report the development of a gravimeter lowered from a vessel [11] and

Ballau et.al. report its deployment on the Juan de Fuca Ridge [2]. While this technique significantly reduces the infrastructure necessary for obtaining on-bottom gravity measurements, uncertainty in the lateral position estimates – approximately 100–200 m [26] – preclude using this technique for precision gravity surveying. This limitation, and that of corruption of the gravity measurements due to vehicle motion, can be overcome by using a gravimeter system designed to sit on the seafloor [24]. Sasagawa and colleagues report the development of a gravimeter, ROVDOG, which is carried to a site by an HOV or remotely operated vehicle (ROV), set on the seafloor using the vehicles manipulator, and measurements obtained. The scientific results of a survey using this gravimeter system and the *Alvin* submersible on the Atlantis Massif are reported in [20].

TABLE I
SUMMARY OF PREVIOUS ON-BOTTOM GRAVITY SURVEYS

Vehicle/Gravimeter	Stations	Dives	Citation
Alvin/L&R Model G	23	5	[18]
Alvin/L&R Model G	41	9	[12]
Shinkai 6500/CG-3	17	4	[5]
Alvin/BGM-3	133	13	[21]
Alvin/BGM-3	16	2	[8]
Alvin/L&R Model G	12	2	[22]
Alvin/ROVDOG	72	4	[20]
Alvin/BGM-3	29	3	[9]

On-bottom gravity surveying using point measurements provides valuable observations, however obtaining these measurements is a lengthy process requiring approximately 10 minutes to measure the gravity anomalies, and in the case of stationary gravimeters another 5-10 minutes to stabilize the gravimeter. The time necessary to obtain measurements, coupled with transit time between stations, severely limits the number of measurements taken during a dive. Table 1 summarizes some recent on-bottom gravity surveys. Gravimeters mounted inside an HOV average between 5-10 stations per dive. Employing the ROVDOG system increases the number of stations to 18 per dive. While these measurements obtain valuable gravimetric data, the necessity to continually land the vehicle and then measure gravity precludes surveying even modestly sized areas (e.g., 1000 meters by 1000 meters) with the spatial resolution necessary to locate and map small-scale crustal features.

The number of measurements can be significantly increased with continuous surveying where gravity is measured from a moving submersible operating near the seafloor. Zumberge et al. developed a towed marine gravimeter system, TOWDOG, that is towed approximately 30m off the seafloor and possesses a repeatability of a few tenths of a mGal [32]. Towed gravity surveys possess a number of deficiencies including the necessity to maintain a safe altitude, limited maneuverability, coupling of the tow sled and surface ship motion, and the inability to obtain visual observations of the seafloor that can be correlated to the gravity measurements.

Another continuous technique that allows near-source measurements employs a gravimeter designed for surface ships mounted inside an HOV. The HOV conducts a gravity survey underway, continuously acquiring gravity measurements. This technique has been employed on the Alvin submersible twice on the Eastern Pacific Rise (EPR) – first in 1995 [3] and again in 2000 [28]. The 1995 survey possessed a repeatability of approximately 0.3 mGal and along-track spatial resolutions of approximately 130160 m. Data obtained at the EPR 9°50'N ridge axis suggests that dike swarms contribute to the gravity anomalies. The 2000 survey benefited from the addition of Doppler sonar velocity measurements, and the spatial resolution was improved to approximately 100m. While this spatial resolution represents a significant improvement, it is insufficient for resolving fine-scale features in the shallow crust.

A. Challenges of Underway Gravity Surveying

The primary obstacle to continuous gravity surveying is the vertical acceleration measured by the gravimeter due to the vehicle's motion – i.e., the vertical component of the vehicle induced gravimeter acceleration (VIGA). When deployed on a submersible underway, the gravimeter measures gravitational forces typically measured by stationary gravimeters plus the accelerations resulting from the motion of the vehicle. Obtaining precision gravity measurements with this technique requires accurately estimating the vertical component of the VIGA such that it can be explicitly subtracted from the gravity measurements [Cochran et al., 1999]. The vertical VIGA, ${}^{w}\ddot{p}_{g_z}$, is related to the vehicle's state (i.e., position and velocity) by the equation (see appendix for derivation):

$$ {}^{w}\ddot{p}_{g_z} = \dot{J}_1\dot{\theta} + \dot{J}_2\dot{\psi} + J_1\ddot{\theta} + J_2\ddot{\psi} + {}^{w}\ddot{p}_{v_z} \qquad (1) $$

where: ${}^{w}\ddot{p}_{v_z}$ is the vehicle's vertical acceleration; $\dot{\theta}$ and $\dot{\psi}$ are the first derivatives with respect to time of pitch and roll (θ and ψ respectively); $\ddot{\theta}$ and $\ddot{\psi}$ are the second derivatives with respect to time of pitch and roll; and $J_1, J_2, \dot{J}_1$, and $\dot{J}_2$ are functions defined in the appendix. The first term is the *translational* component of the vertical VIGA, while the latter terms represent the vertical VIGA resulting from the vehicle's *rotational* motion. Obtaining accurate estimates of vertical VIGA enables explicitly subtracting it from the gravity measurements, thereby improving the precision of the measurements. Consequently, continuous fine-spatial gravity surveying requires (i) minimizing the vehicles vertical and rotational motions; and (ii) obtaining accurate estimates of the residual vertical component of the VIGA, thereby enabling us to explicitly subtract it from the gravity measurements.

III. Gravity Surveying with Autonomous Underwater Vehicles

Mounting a gravimeter on a vehicle possessing minimal depth and attitude motions significantly reduces the vertical VIGA. Previous continuous near-bottom gravity surveys (e.g., [3], [28], [32]) have employed human operated vehicles (HOVs) or tow sleds, however, in the context of gravity surveying, AUVs possess two distinct advantages over HOVs. AUVs employ thrusters and/or control surfaces to automatically control the depth of the vehicle to within a few centimeters (e.g., [29], [30]) – a capability presently not available on the *Alvin* HOV or tow sleds. Furthermore, AUVs possessing a high separation between the center of buoyancy and the center of gravity are more stable in attitude than ROVs and HOVs. The superior attitude stability of this class of AUVs is demonstrated in Figure 3 (originally published in [6]). The figure compares the pitch and roll of the *Alvin* HOV, *Jason 2* ROV, and the *ABE* AUV during constant heading tracklines. The attitude stability of AUVs and their ability to maintain precision depth significantly reduces the vertical VIGA. The dynamic performance of AUVs, combined with their ability of to efficiently survey large areas of the seafloor (i.e., [30], [19], [17]), make them ideal platforms for gravity surveying. To date, AUV gravimetry has only been briefly discussed in the literature [1] and limited laboratory testing has been done [7].

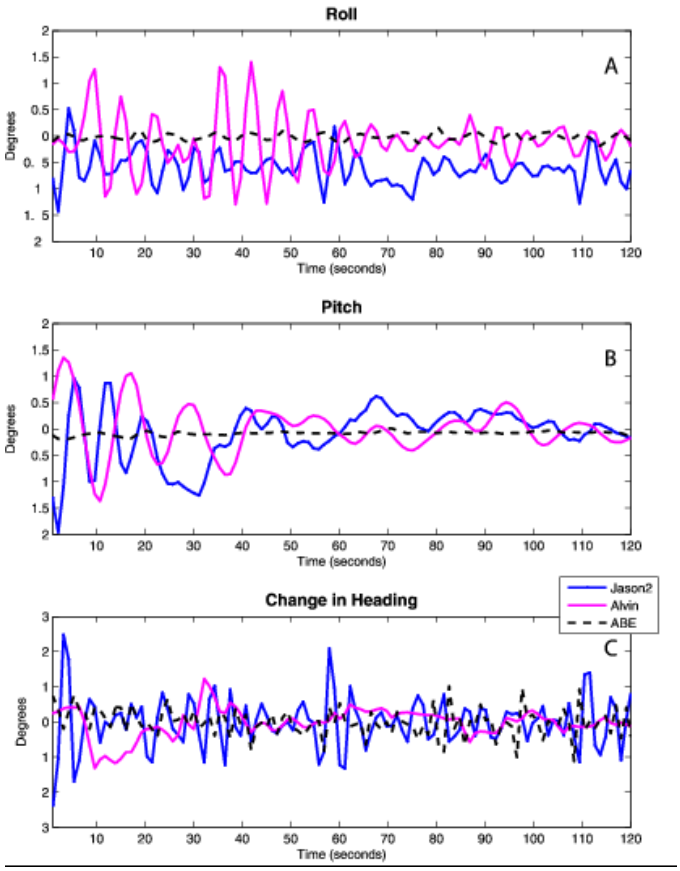

Fig. 3. Plots of the vehicle roll (top), pitch (middle), and change in heading (bottom) for *Alvin*, the *Jason 2* ROV, and the *ABE* AUV (line colors are magenta, blue, and black, respectively). The increased pitch and roll stability of the *ABE* AUV compared to *Alvin* and *Jason 2* demonstrates the vehicle dynamics advantages of using AUVs for gravity surveying. Plot originally published in [6].

IV. On-Bottom versus Underway Gravimetry

Identifying the limits of the gravity measurement and spatial resolution achievable from a moving submersible is a key challenge in gravity surveying. The on-bottom technique minimizes vehicle motion and reduces the distance between the gravimeter and the gravity anomaly source, however operating an autonomous vehicle close to the seafloor is difficult. Measuring gravity while moving 5-10 meters off the seafloor simplifies vehicle operations, however it requires that vehicle accelerations be decoupled from the measured

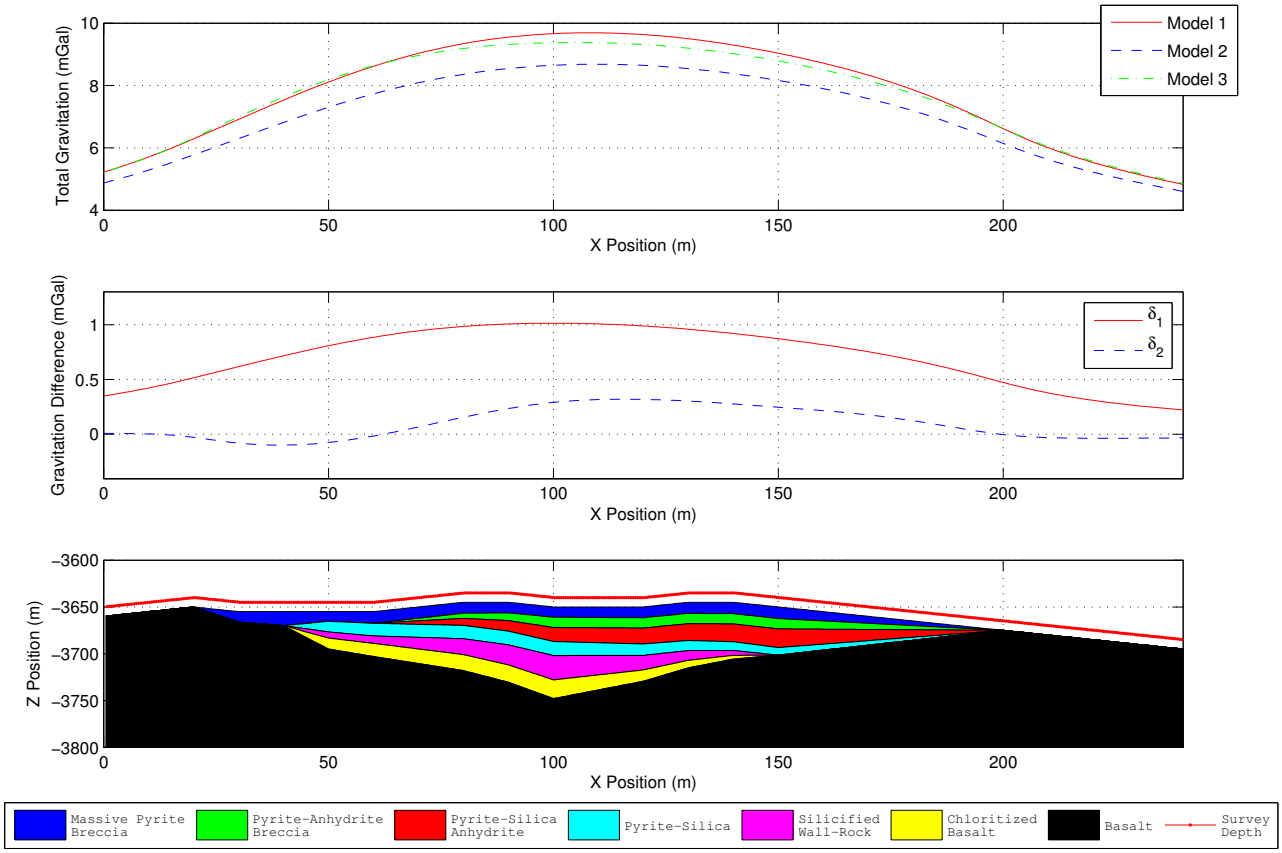

Fig. 4. Top: The gravity field anomaly resulting from the presence of sulfides underneath the TAG mound. The lower plot is a cross-section of the TAG mound showing the six metal-rich sulfide layers based on data obtained from Ocean Drilling Program Leg 158 in 1994 [14]. The sulfides possess a higher density than the surrounding basalt, resulting in an increased gravity field anomaly.

gravity, while the increased distance from the gravity anomaly source to the gravimeter decreases the measured gravity anomaly (the inverse quadratic distance acts as a low-pass filter). The operational simplicity of continuous surveying makes it the preferred technique for obtaining gravity measurements, however the small amplitude (less than 1 mGal) gravity signals of small-scale geophysical features often requires measuring gravity from a stationary vehicle close to the gravity anomaly. This section discusses limitations on underway gravity measurements, based on vehicle control and state sensing.

To better understand the impact of these limitations on gravity surveys, we developed a gravity model for a cross-section of the TAG hydrothermal mound located in the rift valley of the North Atlantic MOR. The lower plot in Figure 4 shows the cross-section of the sub-seafloor crust based on drill cores obtained during Ocean Drilling Program cruise 158 in 1994 [14]. The crust immediately beneath the TAG mound contains six metal-rich sulfide layers of differing density and porosity (Table II) with the ambient basalt underneath and surrounding these layers. We simulated the gravity anomaly resulting from different crustal structures based on a constant altitude survey 10m off the seafloor. The upper plot in Figure 4 shows the gravity field anomaly resulting from three models:

1) gravity anomaly resulting from the presence of the mineral sulfides in the shallow oceanic crust;
2) the gravity anomaly created if the mound contained *no sulfides* (i.e., was comprised solely of basalt); and
3) the top layer of massive pyrite breccia is 10m thinner than in case (1) and the volume is replaced with a 10m thicker layer of pyrite-anhydrite breccia. Since the pyrite-anhydrite breccia is of lower density than the massive pyrite breccia, the gravity anomaly for case (3) is less than that for case (1). This case illustrates how gravity measurements can be used to resolve the size and composition of

small-scale features in the oceanic crust.

The middle plot shows the difference in the gravity anomaly between models 1 and 2 (δ_1 represented by the solid red line) and models 1 and 3 (δ_2 represented by the dashed green line).

TABLE II
LAYER DENSITY AND POROSITY VALUES

Layer	Density	Porosity
	kg/m^3	%
Massive-Pyrite Breccia	3625	6.88
Pyrite-Anhydrite Breccia	3350	10.49
Pyrite-Silica Anhydrite	3625	11.82
Pyrite-Silica	3240	10.49
Silicified Wall-rock	3440	5.04
Chloritized Basalt	3490	4.89
Basalt	2880	1.44

The two cases in the middle plot of 4 help answer two key geophysical questions — δ_1 helps geophysicists *detect* the presence of sulfides in the shallow oceanic crust, while the gravity data in δ_2 provides scientists with additional information with which they can *investigate* the extent (i.e., the size and geometry) of the sulfides. The detection case (δ_1) is a gravity anomaly difference of up to 1.1 mGal over a distance of 240m. — large enough to be detected during an underway gravity survey [3], [28]. More difficult is the investigation case of obtaining sub-mGal spatially-dense gravity measurements shown in δ_2. The remainder of this section discusses some practical limitations on the ability of AUVs to obtain the high-resolution, spatially-dense measurements underway.

A. Precision Depth Control

Essential to underway gravity measurements is the ability to control vehicle depth. Consider the following simple analysis. A vehicle moving at $v_f = 0.5m/s$ will induce a 1mGal centripetal acceleration (a_c) over an arc-radius (r) of

$$r = \frac{v_f^2}{a_c} \quad (2)$$
$$= (0.5m/s)^2/(10^5 m/s^2) \quad (3)$$
$$= 25000m. \quad (4)$$

If the vehicle traveled 100m horizontally, the resulting change in depth (δz) would be

$$\delta z = r - (r^2 - 100^2)^{0.5} \quad (5)$$
$$= 0.2m. \quad (6)$$

Consequently, to keep the centripetal acceleration within 1mGal, the vehicle would have to hold depth to within 0.2m. For the 0.1mGal case, the necessary depth control precision is 0.02m. AUVs are currently capable of achieving the former 0.2m (1mGal) specification, however controlling depth to with 0.02m exceeds the capabilities of AUV depth controllers.

B. Attitude and Depth Estimation Accuracy

Equation (1) demonstrates the need to accurately estimate the attitude and vertical (depth) state of the vehicle Underway gravity surveys require commercially available fiber-optic gyroscopes (FOGs) capable of measuring attitude and attitude rates with the accuracy necessary to subtract the vertical VIGA from the gravimeter measurements. In addition, previously reported continuous gravity surveys [3], [32] employed double-differentiated vehicle depth measurements to estimate the translational component, ${}^w\ddot{p}_{v_z}$. By combining depth measurements with DVL velocity data and model-based state estimators (e.g., [16], [23]), the accuracy of the vehicle's vertical acceleration (${}^w\ddot{p}_{v_z}$) can be further improved.

C. Heading Sensing Accuracy

Obtained gravity data must undergo a number of corrections to obtain scientifically meaningful data. Among the corrections is the Eötvös effect, a function of vehicle velocity and heading. The Eötvös effect is a consequence of the motion of an object relative to the motion of the earth. For a submersible conducting a gravity survey, moving eastward reduces measured gravity while a westward moving vehicle measures an increased gravity. This is a result of centripetal acceleration due to the vehicle's motion relative to the earth's rotation and is expressed as:

$$g_e = 7.503 v_f cos(\mu) sin(\phi) + 0.004154 v_f^2 \quad (7)$$

where v_f is the forward speed of the vehicle in knots; μ is the latitude in radians, and ϕ is the vehicle heading in radians.

The dependency of the Eötvös effect correction on the heading and velocity navigation sensors implies that these sensors must possess sufficient accuracy in order to correctly compensate for the

Eötvös effect. Figure 5 shows the Eötvös effect error for a series of different heading errors for a vehicle moving due East ($90°$) at $45°$ latitude as a function of forward velocity. Heading sensors possessing superior accuracy, such as fiber-optic gyroscopes, enable correcting the Eötvös effect to a higher accuracy than lower quality heading sensors.

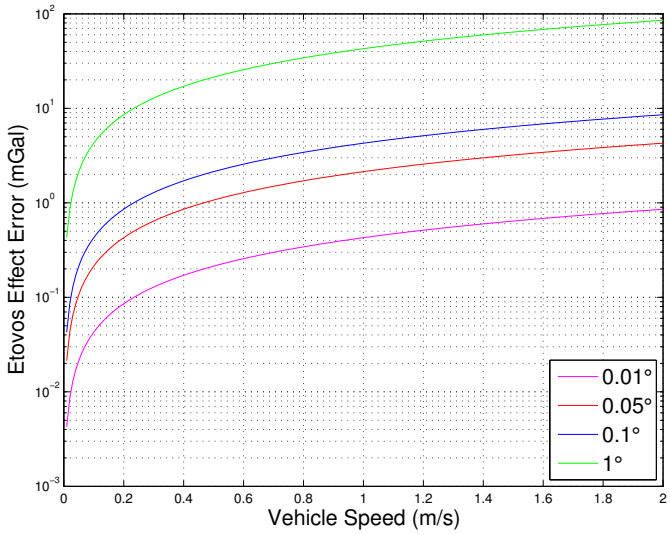

Fig. 5. Error in the Eötvös effect for a vehicle moving due East ($90°$) at $45°$ latitude resulting from vehicle heading sensor accuracy errors ranging from $0.01°$ to $1°$. Superior heading sensor accuracy implies that gravity measurements obtained by a gravimeter mounted on the vehicle can have the Eötvös effect corrected to a higher resolution, thereby improving the overall accuracy of the gravity measurement. For example, the Eötvös effect error for a vehicle moving East at 1m/s with a heading sensor error of $0.01°$ will be approximately 0.3mGal.

D. Impact of Vehicle Speed on Geophysical Wavelength Detection

Detecting fine-scale features in the shallow oceanic crust, such as dikes, requires obtaining high-resolution gravity measurements with a spatial density equivalent or superior to that of the geophysical feature. For example, detecting a 5m wide dike requires a spatial density of 5m or less. In the context of underway gravity measurements, the spatial density (or wavelength) is a function of the vehicle velocity and the time period over which the gravity measurements are filtered [3]. The wavelength, λ, can be expressed as:

$$\lambda = v_f \tau \tag{8}$$

where v_f is the vehicle's forward velocity and τ is the time period over which the gravity measurements are filtered.

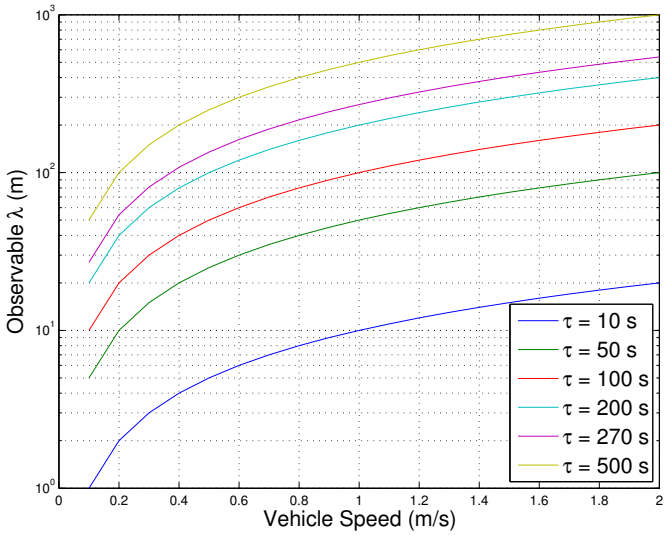

Fig. 6. The observable geophysical wavelength as a function of vehicle velocity for different gravity filter time periods. Measuring small-scale features (e.g., under 10m) requires a short filtering period or slow vehicle speeds.

Figure 6 shows the observable wavelength for a series of filtering periods (τ) as a function of vehicle velocity. Obtaining gravity measurements with low observable wavelengths requires lowering the sample period or reducing vehicle speed. For example, to obtain an observable wavelength of 10m or less with a vehicle moving at 1m/s requires using a filtering gravity data with a 10s period. Alternatively, the vehicle can move at 0.2m/s and a 50s filter period can be used. The trade-off between filter period and vehicle speed is difficult as vehicles employing control surfaces must operate above stall speed, and decreasing the filter period reduces the ability to obtain sub-mGal gravity measurements.

Based on this analysis, we can conclude:

1) High accuracy attitude and heading sensors are essential for *(i)* estimating the vertical VIGA; and *(ii)* correcting for the Eötvös effect. Obtaining sub-mGal gravity measurements at reasonable vehicle speeds (e.g., above 0.2m/s requires heading sensor accuracy greater than $0.1°$).
2) Obtaining sub-mGal gravity measurements requires precision vehicle depth control on the order of centimeters — a capability currently not possessed by most AUVs.
3) Spatially-dense measurements on the order of less than 10m requires either short gravity

filter periods (which compromises the ability to obtain sub-mGal measurements) and/or slow vehicle velocities (which for AUVs with control surfaces limits maneuverability).

Considering these limitations, underway gravity surveys are suited to the *detection* task of finding geophysical features on the order of 1-10mGal. Investigating the extent of geophysical features (typically requiring sub-mGal gravity measurements with spatial-density on the order of 1-10m) from a moving vehicle requires control and state estimation capabilities currently unavailable.

V. Conclusions

This paper discusses the application of AUVs to gravity surveying of geophysical features in the shallow oceanic crust. Previous submerged gravity surveys are reviewed and the challenges of underway gravity surveys discussed. The advantages of on-bottom and underway gravity surveys are presented and limitations on the ability of underway gravity surveys to measure the extent (e.g., size and composition) of geophysical features are identified. Current AUV navigation and control methodologies allow for underway gravity surveying that can detect the presence of features such as mineral sulfide deposits in the shallow ocean oceanic crust. Additional work is necessary to be capable of detecting smaller features. Included in this research is analytical research into improved navigation and gravity filtering techniques, and the development of gravimeters capable of being deployed on AUVs. The scientific benefit of AUV gravimetry extends beyond MORs to include other regions with complex shallow ocean crustal structure and will also have an impact on mineral exploration and strategic applications.

References

[1] M. D. Ageev, "AUV-a precise platform for underwater gravity measurement," in *In Proceedings of IEEE OCEANS '94.*, Brest, 1994, vol. 1.

[2] V. S. Ballu, J. A. Hildebrand, and S. C. Webb, "Seafloor gravity evidence for hydrothermal alteration of the sediments in Middle Valley, Juan de Fuca Ridge," *Marine Geology*, vol. 150, no. 1, pp. 99–111, Sept. 1998.

[3] J. R. Cochran, D. J. Fornari, B. J. Coakley, R. Herr, and M. A. Tivey, "Continous near-bottom gravity measurements made with a BGM-3 gravimeter in DSV Alvin on the East Pacific Rise near 9°31'N and 9°50' N," *Journal of Geophysical Research*, vol. 104, no. B5, pp. 10,841 – 10,861, May 1999.

[4] J. R. Delaney, D. S. Kelley, M. D. Lilley, D. A. Butterfield, J. A. Baross, W. S. D. Wilcock, R. W. Embley, and M. Summit, "The quantum event of oceanic crustal accretion: Impacts of diking at mid-ocean ridges," *Science*, vol. 281, no. 5374, pp. 222–230, July 1998.

[5] R. L. Evans, "A seafloor gravity profile across the TAG hydrothermal mound," *Geophysical Research Letters*, vol. 23, no. 23, pp. 3447–3450, 1996.

[6] V. Ferrini, D. Fornari, T. Shank, J. Kinsey, S. Soule, S. Carbotte, M. Tivey, L. Whitcomb, D. Yoerger, and J. Howland, "Sub-meter bathymetric mapping of the East Pacific Rise crest at 9° 50'N linking volcanic and hydrothermal processes," *Geochemisty, Geophysics, Geosystems*, vol. 8, 2007, Q01006.

[7] H. Fujimoto, K. Koizumi, M. Watanabe, A. Oshida, T. Furuta, N. Takamura, and T. Ura, "Underwater gravimeter on board the R-One robot," in *Proceedings of the International Symposium on Underwater Technology*, Tokyo, 2000, pp. 297–300.

[8] L. A. Gilbert and H. P. Johnson, "Direct measurements of oceanic crustal density at the northern Juan de Fuca Ridge," *Geophysical Research Letters*, vol. 26, no. 24, pp. 3633–3636, Dec 1999.

[9] L. A. Gilbert, R. E. McDuff, and H. P. Johnson, "Porosity of the upper edifice of axial seamount," *Geology*, vol. 35, no. 1, pp. 49–52, Jan. 2007.

[10] M. Hannington, I. Jonasson, P. Herzig, , and S. Petersen, *Physical, Chemical, Biological and Geological Interactions within Hydrothermal Systems*, chapter Physical and chemical processes of seafloor mineralization, pp. 115–157, American Geophysical Union, Washington, D.C., 1995.

[11] J. A. Hildebrand, J. M. Stevenson, P. T. C. Hammer, M. A. Zumberge, R. L. Parker, C. G. Fox, and P. J. Meis, "A seafloor and sea-surface gravity survey of axial volcano," *Journal of Geophysical Research-solid Earth and Planets*, vol. 95, no. 8, pp. 12751–12763, 1990.

[12] M. L. Holmes and H. P. Johnson, "Upper crustal densities derived from sea—floor gravity measurements - Northern Juan-de-Fuca Ridge," *Geophysical Research Letters*, vol. 20, no. 17, pp. 1871–1874, Sept. 1993.

[13] M. L. Holmes and H. P. Johnson, "Upper crustal densities derived from sea-floor gravity measurements - northern Juan-de-Fuca Ridge," *Geophysical Research Letters*, vol. 20, no. 17, pp. 1871–1874, Sept. 1993.

[14] S. E. Humphris, P. M. Herzig, D. J. Miller, J. C. Alt, K. Becker, D. Brown, G. Brugmann, H. Chiba, Y. Fouquet, J. B. Gemmell, G. Guerin, M. D. Hannington, N. G. Holm, J. J. Honnorez, G. J. Iturrino, R. Knott, R. Ludwig, K. Nakamura, S. Petersen, A. L. Reysenbach, P. A. Rona, S. Smith, A. A. Sturz, M. K. Tivey, and X. Zhao, "The internal structure of an active sea-floor massive sulfide deposit," *Nature*, vol. 377, no. 6551, pp. 713–716, October 15 1995.

[15] H. P. Johnson, M. Pruis, D. Van Patten, and M. Tivey, "Density and porosity of the upper oceanic crust from seafloor gravity measurements," *Geophysical Research Letters*, vol. 27, no. 7, pp. 1053–1056, 2000.

[16] J. C. Kinsey and L. L. Whitcomb, "Model-based observers for underwater vehicle navigation: Theory and preliminary experiments," in *Proceedings of the IEEE International Conference on Robotics and Automation*, Rome, Italy, April 2007, pp. 4251–4256.

[17] W. Kirkwood, D. Gashler, H. Thomas, T. O'Reilly, R. McEwen, N. Tervalon, F. Shane, D. Au, M. Sibenac, T. Konvalina, A. Bahlavouni, and J. Bellingham, "Development of a long endurance autonomous underwater vehicle for ocean science exploration," in *Oceans Conference Record (IEEE)*, Honolulu, HI, Nov. 2001, vol. 3, pp. 1504–1512.

[18] B. P. Luyendyk, "On-bottom gravity profile across the East Pacific Rise Crest a 21° North," *Geophysics*, vol. 49, no. 12, pp. 2166–2177, 1984.

[19] K. Nicholls, E. Abrahamsen, J. Buck, P. Dodd, C. Goldblatt, G. Griffiths, K. Heywood, N. Hughes, A. Kaletzky, G. Lane-Serff, S. McPhail, N. Millard, K. Oliver, J. Perrett, M. Price, C. Pudsey, K. Saw, K. Stansfield, M. Stott, P. Wadhams, A. Webb, and J. Wilkinson, "Measurements beneath an Antarctic ice shelf using an autonomous underwater vehicle," *Geophysical Research Letters*, vol. 33, no. 8, Apr. 2006.

[20] S. L. Nooner, G. S. Sasagawa, D. K. Blackman, and M. A. Zumberge, "Structure of oceanic core complexes: Constraints from seafloor gravity measurements made at the Atlantis Massif," *Geophysical Research Letters*, vol. 30, no. 8, pp. 29–1, Apr. 2003.

[21] M. J. Pruis and H. P. Johnson, "Porosity of very young oceanic crust from sea floor gravity measurements," *Geophysical Research Letters*, vol. 25, no. 11, pp. 1959–1962, June 1998.

[22] M. J. Pruis and H. P. Johnson, "Age dependent porosity of young upper oceanic crust: Insights from seafloor gravity studies of recent volcanic eruptions," *Geophysical Research Letters*, vol. 29, no. 5, pp. 20–1, Mar. 2002.

[23] J. E. Refsnes, K. Y. Pettersen, and A. J. Sørensen, "Observer design for underwater vehicles with position and angle measurement," in *7th IFAC Conference on Manoeuvring and Control of Marine Craft*, Lisbon, Portugal, September 2006.

[24] G. S. Sasagawa, W. Crawford, O. Eiken, S. Nooner, T. Stenvold, and M. A. Zumberge, "A new sea-floor gravimeter," *Geophysics*, vol. 68, no. 2, pp. 544–553, 2003.

[25] M. W. Spong and M. Vidyasagar, *Robot Dynamics and Control*, Wiley, New York, 1989.

[26] J. M. Stevenson, J. A. Hildebrand, M. A. Zumberge, and C. G. Fox, "An ocean-bottom gravity study of the Southern Juan-de-Fuca Ridge," *Journal of Geophysical Research-solid Earth*, vol. 99, no. 3, pp. 4875–4888, 1994.

[27] M. A. Tivey and H. P. Johnson, "Crustal magnetization reveals subsurface structure of Juan de Fuca Ridge hydrothermal vent fields," *Geology*, vol. 30, no. 11, pp. 979–982, 2002.

[28] D. Yoerger, J. Cochran, D. Fornari, R. Herr, T. McGee, H. Schouten, and M. Tivey, "Near-bottom, underway gravity survey of the small overlapping spreading center at 9° 37'N on the East Pacific Rise Crest," in *Eos Trans. AGU 81(48), Fall Meet. Suppl.*, 2000, Abstract T51D-16.

[29] D. R. Yoerger, A. M. Bradley, B. B. Walden, H. Singh, and R. Bachmayer, "Surveying a subsea lava flow using the Autonomous Benthic Explorer (ABE)," *International Journal of Systems Science*, vol. 29, no. 4, pp. 1031–1044, October 1998.

[30] D. R. Yoerger, M. Jakuba, A. M. Bradley, and B. Bingham, "Techniques for deep sea near bottom survey using an autonomous underwater vehicle," *International Journal of Robotics Research*, vol. 26, no. 1, pp. 41–54, January 2007.

[31] R. A. Zierenberg, Y. Fouquet, D. J. Miller, J. M. Bahr, P. A. Baker, T. Bjerkgard, C. A. Brunner, R. C. Duckworth, R. Gable, J. Gieskes, W. D. Goodfellow, H. M. Groschel-Becker, G. Guerin, J. Ishibashi, G. Iturrino, R. H. James, K. S. Lackschewitz, L. L. Marquez, P. Nehlig, J. M. Peter, C. A. Rigsby, P. Schultheiss, W. C. Shanks, B. R. T. Simoneit, M. Summit, D. A. H. Teagle, M. Urbat, and G. G. Zuffa, "The deep structure of a sea-floor hydrothermal deposit," *Nature*, vol. 392, no. 6675, pp. 485–488, Apr. 1998.

[32] M. A. Zumberge, J. R. Ridgway, and J. A. Hildebrand, "A towed marine gravity meter for near-bottom surveys," *Geophysics*, vol. 62, no. 5, pp. 1386–1393, 1997.

APPENDIX

Definition: ${}^{w}p_v \in R^3$, is the XYZ position of the origin of the vehicle in the world frame, i.e.,

$$ {}^{w}_{}p_v = \begin{bmatrix} {}^{w}p_{v_x} \\ {}^{w}p_{v_y} \\ {}^{w}p_{v_z} \end{bmatrix}. \tag{10} $$

In this application, the vehicle frame origin is assumed to be the center of rotation of the vehicle.

Definition: ${}^{w}p_g \in R^3$, is the XYZ position of the gravimeter in the world frame, i.e.,

$$ {}^{w}_{}p_g = \begin{bmatrix} {}^{w}p_{g_x} \\ {}^{w}p_{g_y} \\ {}^{w}p_{g_z} \end{bmatrix}. \tag{11} $$

Definition: The heading (ϕ), pitch (θ), and roll (ψ) of the vehicle can be represented as a rotation matrix [25] ${}^{g}_{v}R \in SO(3)$ defined in (9).

Definition: ${}^{g}_{v}d \in R^3$ is vector representing the XYZ distance from the origin of the vehicle frame to the origin of the gravimeter frame, i.e.,

$$ {}^{g}_{v}d = \begin{bmatrix} {}^{g}_{v}d_x \\ {}^{g}_{v}d_y \\ {}^{g}_{v}d_z \end{bmatrix}. \tag{12} $$

This offset is a measured constant.

Knowing ${}^{w}p_v$, ${}^{g}_{v}R$, and ${}^{g}_{v}d$ we can compute the position of the gravimeter, ${}^{w}p_g$, to be:

$$ {}^{w}_{}p_g = {}^{g}_{v}R\,{}^{g}_{v}d + {}^{w}_{}p_v \tag{13} $$

$$. \tag{14} $$

The derivative of ${}^{w}p_g$ with respect to time (i.e., $\frac{d\,{}^{w}p_g}{dt}$) is:

$$ {}^{w}_{}\dot{p}_g = J \begin{bmatrix} {}^{w}\dot{p}_{v_x} \\ {}^{w}\dot{p}_{v_y} \\ {}^{w}\dot{p}_{v_x} \\ \dot{\phi} \\ \dot{\theta} \\ \dot{\psi} \end{bmatrix}. \tag{15} $$

$J(p, r, d)$ is the Jacobian and is defined as:

$$ J = \begin{bmatrix} \frac{\partial\,{}^{w}p_{g_x}}{\partial\,{}^{w}p_{v_x}} & \frac{\partial\,{}^{w}p_{g_y}}{\partial\,{}^{w}p_{v_x}} & \frac{\partial\,{}^{w}p_{g_z}}{\partial\,{}^{w}p_{v_x}} \\ \frac{\partial\,{}^{w}p_{g_x}}{\partial\,{}^{w}p_{v_y}} & \frac{\partial\,{}^{w}p_{g_y}}{\partial\,{}^{w}p_{v_y}} & \frac{\partial\,{}^{w}p_{g_z}}{\partial\,{}^{w}p_{v_y}} \\ \frac{\partial\,{}^{w}p_{g_x}}{\partial\,{}^{w}p_{v_z}} & \frac{\partial\,{}^{w}p_{g_y}}{\partial\,{}^{w}p_{v_z}} & \frac{\partial\,{}^{w}p_{g_z}}{\partial\,{}^{w}p_{v_z}} \\ \frac{\partial\,{}^{w}p_{g_x}}{\partial\phi} & \frac{\partial\,{}^{w}p_{g_y}}{\partial\phi} & \frac{\partial\,{}^{w}p_{g_z}}{\partial\phi} \\ \frac{\partial\,{}^{w}p_{g_x}}{\partial\theta} & \frac{\partial\,{}^{w}p_{g_y}}{\partial\theta} & \frac{\partial\,{}^{w}p_{g_z}}{\partial\theta} \\ \frac{\partial\,{}^{w}p_{g_x}}{\partial\psi} & \frac{\partial\,{}^{w}p_{g_y}}{\partial\psi} & \frac{\partial\,{}^{w}p_{g_z}}{\partial\psi} \end{bmatrix}^T \tag{16} $$

$$ {}^{g}_{v}R = \begin{bmatrix} c(\phi)c(\theta) & -s(\phi)c(\psi)+c(\phi)s(\theta)s(\psi) & s(\phi)s(\psi)+c(\phi)s(\theta)c(\psi) \\ s(\phi)c(\theta) & c(\phi)c(\psi)+s(\phi)s(\theta)s(\psi) & -c(\phi)s(\psi)+s(\phi)s(\theta)c(\psi) \\ -s(\theta) & c(\theta)s(\psi) & c(\theta)c(\psi) \end{bmatrix} \tag{9} $$

The vertical acceleration of the gravimeter is the derivative with respect to time of 15:

$$ {}^{w}\ddot{p}_{g} = \frac{d}{dt} J \begin{bmatrix} {}^{w}\dot{p}_{v_x} \\ {}^{w}\dot{p}_{v_y} \\ {}^{w}\dot{p}_{v_x} \\ \dot{\phi} \\ \dot{\theta} \\ \dot{\psi} \end{bmatrix} \tag{17} $$

$$ = \dot{J} \begin{bmatrix} {}^{w}\dot{p}_{v_x} \\ {}^{w}\dot{p}_{v_y} \\ {}^{w}\dot{p}_{v_x} \\ \dot{\phi} \\ \dot{\theta} \\ \dot{\psi} \end{bmatrix} + J \begin{bmatrix} {}^{w}\ddot{p}_{v_x} \\ {}^{w}\ddot{p}_{v_y} \\ {}^{w}\ddot{p}_{v_x} \\ \ddot{\phi} \\ \ddot{\theta} \\ \ddot{\psi} \end{bmatrix} \tag{18} $$

where:

$$ \dot{J} = \begin{bmatrix} \frac{d}{dt}\frac{\partial\ {}^{w}p_{g_x}}{\partial\ {}^{w}p_{v_x}} & \frac{d}{dt}\frac{\partial\ {}^{w}p_{g_y}}{\partial\ {}^{w}p_{v_x}} & \frac{d}{dt}\frac{\partial\ {}^{w}p_{g_z}}{\partial\ {}^{w}p_{v_x}} \\ \frac{d}{dt}\frac{\partial\ {}^{w}p_{g_x}}{\partial\ {}^{w}p_{v_y}} & \frac{d}{dt}\frac{\partial\ {}^{w}p_{g_y}}{\partial\ {}^{w}p_{v_y}} & \frac{d}{dt}\frac{\partial\ {}^{w}p_{g_z}}{\partial\ {}^{w}p_{v_y}} \\ \frac{d}{dt}\frac{\partial\ {}^{w}p_{g_x}}{\partial\ {}^{w}p_{v_z}} & \frac{d}{dt}\frac{\partial\ {}^{w}p_{g_y}}{\partial\ {}^{w}p_{v_z}} & \frac{d}{dt}\frac{\partial\ {}^{w}p_{g_z}}{\partial\ {}^{w}p_{v_z}} \\ \frac{d}{dt}\frac{\partial\ {}^{w}p_{g_x}}{\partial\phi} & \frac{d}{dt}\frac{\partial\ {}^{w}p_{g_y}}{\partial\phi} & \frac{d}{dt}\frac{\partial\ {}^{w}p_{g_z}}{\partial\phi} \\ \frac{d}{dt}\frac{\partial\ {}^{w}p_{g_x}}{\partial\theta} & \frac{d}{dt}\frac{\partial\ {}^{w}p_{g_y}}{\partial\theta} & \frac{d}{dt}\frac{\partial\ {}^{w}p_{g_z}}{\partial\theta} \\ \frac{d}{dt}\frac{\partial\ {}^{w}p_{g_x}}{\partial\psi} & \frac{d}{dt}\frac{\partial\ {}^{w}p_{g_y}}{\partial\psi} & \frac{d}{dt}\frac{\partial\ {}^{w}p_{g_z}}{\partial\psi} \end{bmatrix}^{T} . \tag{19} $$

Only the vertical component of the VIGA is required, thus obviating the need to compute the partial derivatives in the upper two rows of J and $\dot{J}$. Using the required terms of J and $\dot{J}$ computed below, the last row of (18) is:

$$ {}^{w}\ddot{p}_{g_z} = \dot{J}_1\dot{\theta} + \dot{J}_2\dot{\psi} + J_1\ddot{\theta} + J_2\ddot{\psi} + {}^{w}\ddot{p}_{v_z} \tag{20} $$

where:

$$ \begin{aligned} J_1 &= -c(\theta)\ {}^{g}_{v}d_x - s(\theta)s(\psi)\ {}^{g}_{v}d_y + s(\theta)c(\psi)\ {}^{g}_{v}d_z \\ J_2 &= c(\theta)c(\psi)\ {}^{g}_{v}d_y - s(\psi)c(\psi)\ {}^{g}_{v}d_z \\ \dot{J}_1 &= -c(\theta)\ {}^{g}_{v}d_x - s(\theta)s(\psi)\ {}^{g}_{v}d_y + s(\theta)c(\psi)\ {}^{g}_{v}d_z \\ \dot{J}_2 &= c(\theta)c(\psi)\ {}^{g}_{v}d_y - s(\psi)c(\psi)\ {}^{g}_{v}d_z \end{aligned} $$